Official journal of the American Society of Gene & Cell Therapy

MTOpen

original article

MiR-298 Counteracts Mutant Androgen Receptor Toxicity in Spinal and Bulbar Muscular Atrophy

Naemeh Pourshafie[1], Philip R Lee[2], Ke-lian Chen[1], George G Harmison[1], Laura C Bott[1,3], Masahisa Katsuno[4], Gen Sobue[4,5], Barrington G Burnett[6], Kenneth H Fischbeck[1] and Carlo Rinaldi[1,7]

[1]Neurogenetics Branch, National Institute of Neurological Disorders and Stroke, National Institutes of Health, Bethesda, Maryland, USA; [2]Section on Nervous System Development and Plasticity, The Eunice Kennedy Shriver National Institute of Child and Human Development, National Institutes of Health, Bethesda, Maryland, USA; [3]Department of Cell and Molecular Biology, Karolinska Institutet, Stockholm, Sweden; [4]Department of Neurology, Nagoya University Graduate School of Medicine, Nagoya, Japan; [5]Brain and Mind Research Center, Nagoya University Graduate School of Medicine, Nagoya, Japan; [6]Department of Anatomy, Physiology and Genetics, Uniformed Services University of the Health Sciences, F. Edward Hebert School of Medicine, Bethesda, Maryland, USA; [7]Department of Physiology, Anatomy and Genetics, University of Oxford, Oxford, UK

Spinal and bulbar muscular atrophy (SBMA) is a currently untreatable adult-onset neuromuscular disease caused by expansion of a polyglutamine repeat in the androgen receptor (AR). In SBMA, as in other polyglutamine diseases, a toxic gain of function in the mutant protein is an important factor in the disease mechanism; therefore, reducing the mutant protein holds promise as an effective treatment strategy. In this work, we evaluated a microRNA (miRNA) to reduce AR expression. From a list of predicted miRNAs that target human AR, we selected microRNA-298 (miR-298) for its ability to downregulate AR mRNA and protein levels when transfected in cells overexpressing wild-type and mutant AR and in SBMA patient-derived fibroblasts. We showed that miR-298 directly binds to the 3′-untranslated region of the human AR transcript, and counteracts AR toxicity *in vitro*. Intravenous delivery of miR-298 with adeno-associated virus serotype 9 vector resulted in efficient transduction of muscle and spinal cord and amelioration of the disease phenotype in SBMA mice. Our findings support the development of miRNAs as a therapeutic strategy for SBMA and other neurodegenerative disorders caused by toxic proteins.

Received 24 August 2015; accepted 4 January 2016; advance online publication 9 February 2016. doi:10.1038/mt.2016.13

INTRODUCTION

Spinal and bulbar muscular atrophy (SBMA, Kennedy's disease; OMIM #313200) is one of at least nine human neurodegenerative conditions caused by expansion of CAG repeats encoding extended polyglutamine tracts.[1] In SBMA, as in the other polyglutamine diseases, toxicity likely arises from a mechanism of toxic gain of function of the mutant protein.[2] Cell death ultimately results from disruption of multiple cellular processes, including transcription, axonal transport, and mitochondrial function.[3–7] No disease-modifying treatment is currently available for these disorders.

In recent years, gene silencing with antisense oligonucleotides or RNA interference (RNAi) has shown potential for the treatment of polyglutamine diseases and other disorders caused by toxic proteins. In this work, we developed a therapeutic strategy using microRNA (miRNA) to reduce AR expression in muscle and motor neurons. MiRNAs are a class of small noncoding RNAs that regulate expression levels of target mRNAs, usually by suppressing their translation.[8] Increasing evidence indicates that miRNAs play an important role in many aspects of biology[9] and contribute to a variety of human diseases ranging from cancer[10] to neurodegeneration.[11–14] MiR196a overexpression has recently been shown to have benefit in SBMA models,[15] a result that was indirectly achieved by silencing CELF2, a RNA-binding protein implicated in the regulation of post-transcriptional events.

Here, we identified a miRNA that directly targets human AR mRNA, miR-298 (accession number MIMAT0004901),[16] and we found that it suppresses AR protein levels in cell culture and in a SBMA mouse model. Viral delivery of miR-298 with an adeno-associated virus (AAV)9 vector resulted in efficient transduction of muscle and spinal cord and significantly ameliorated disease manifestations in SBMA mice. Our findings support the development of treatments aimed at reducing AR levels and viral delivery of miRNA as a therapeutic strategy for SBMA and other polyglutamine diseases.

RESULTS

MiR-298 suppresses AR expression by directly binding the 3′UTR of the mRNA and counteracts AR toxicity *in vitro*

We sought to test a miRNA approach to directly target AR expression. From a list of predicted miRNAs that target human AR 3′UTR drawn up using the miRWalk database[17] and other prediction tools (miRanda, miRDB, Targetscan) (**Supplementary** Table S1), we tested the top candidates for their ability to downregulate AR when transfected in a human cell line endogenously expressing AR (**Supplementary Figure S1**). Among those, we selected miR-298 (GFCh38: NC_000020.11; chr20:58818226-58818313)

Correspondence: Carlo Rinaldi, Department of Physiology, Anatomy and Genetics, Le Gros Clark Building, Room 114, University of Oxford, South Parks Rd, Oxford OX1 3QX, UK. E-mail: carlo.rinaldi@dpag.ox.ac.uk

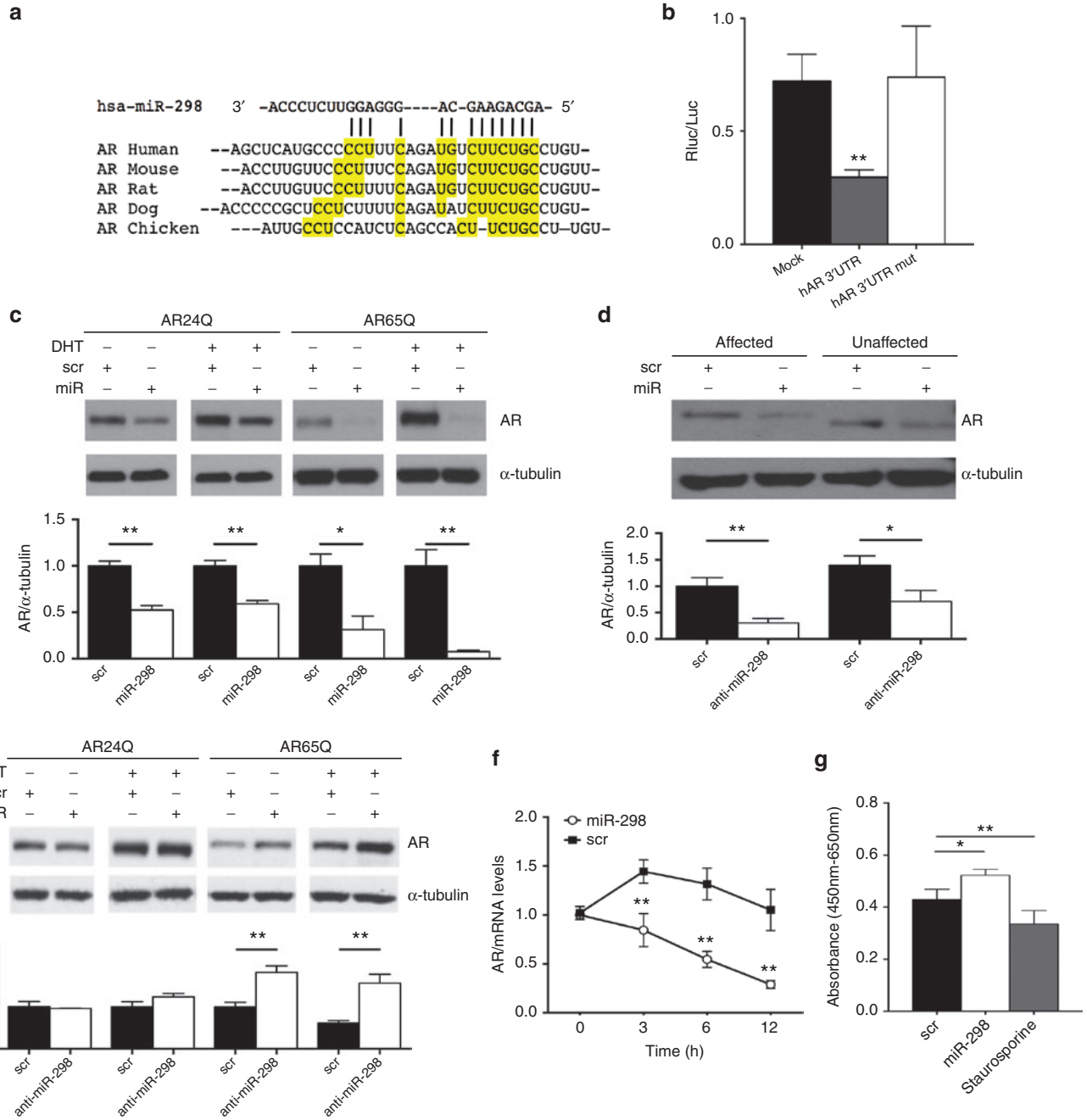

Figure 1 MiR-298 suppresses AR mRNA and protein levels by directly binding to the 3′-UTR region and counteracts AR toxicity *in vitro*. (**a**) Multiple sequence alignment of miR-298 seed region in the 3′UTR of human AR. (**b**) MCF7 cells were cotransfected with miR-298 and empty vector (mock), a construct containing the first 4,000 bp of wild-type human AR 3′UTR (hAR 3′UTR) and the same construct with mutations in the seed region (hAR 3′UTR mut) for the renilla-luciferase assay. $^{**}P < 0.01$. (**c**) Western blot and densitometric analyses showing AR protein expression in AR24Q and AR65Q MN1 cells that had been treated with miR-298 (miR) or scrambled control (scr), in presence of dihydrotestosterone (DHT) (10 nmol/l) or ethanol. AR was detected with H-280 antibody. α-tubulin is shown as loading control ($n = 5$). $^{*}P < 0.05$, $^{**}P < 0.01$. (**d**) Western blot and densitometric analyses showing AR protein expression in human fibroblasts from an affected and an unaffected subject that had been treated with miR-298 (miR) or scrambled control (scr), in presence of DHT (10 nmol/l) or ethanol. AR was detected with H-280 antibody. α-tubulin is shown as loading control ($n = 3$). $^{*}P < 0.05$, $^{**}P < 0.01$. (**e**) Western blot and densitometric analyses showing AR protein expression in AR24Q and AR65Q MN1 cells that had been treated with anti-miR-298 (anti-miR) or scrambled control (scr), in presence of DHT (10 nmol/l) or ethanol. AR was detected with H-280 antibody. α-tubulin is shown as loading control ($n = 5$). $^{**}P < 0.01$. (**f**) AR expression was assessed by real-time reverse transcription-PCR (qRT-PCR) using total RNA extracted from MCF7 cells treated with actinomycin D and miR-298 or scramble for the indicated times ($n = 5$). $^{**}P < 0.01$. (**g**) Viability of AR65Q MN1 cells treated with miR-298, scrambled control (scr), or staurosporine was measured by XTT assay. $^{*}P < 0.05$, $^{**}P < 0.01$.

because it had the highest efficacy in reducing AR protein levels (**Supplementary Figure S1**). The predicted miR-298 binding sites in the 3′UTR of AR, together with the flanking sequence, are conserved across species as shown by the multiple sequence alignment (**Figure 1a**). Direct binding of miR-298 to the putative seed region on the AR 3'UTR was tested with a luciferase assay system. Co-transfection of miR-298 and a construct containing the first 4 kb of the AR 3'UTR yielded more than 65% decrease in reporter activity compared to vector alone. The effect was lost when the miRNA target site was mutated (**Figure 1b**). To validate the effect of miR-298 on AR levels, we used murine motor neuron-neuroblastoma (MN1) cells stably transfected with nonexpanded (AR24Q) or pathologically-expanded (AR65Q) polyglutamine tract in the human AR.[18] The predicted region of binding is present within the first 50 bases of the AR 3'UTR and is included in the transgenes. Forty-eight hours after transfection with a miR-298 mimic, AR protein levels were significantly decreased both in the presence and absence of the ligand dihydrotestosterone (DHT) (**Figure 1c**). In the presence of DHT, the reduction was up to 45% for AR24Q and 80% for AR65Q (**Figure 1c**). We next investigated the effect of miR-298 on endogenous AR protein levels in fibroblasts obtained from a healthy control and from an SBMA patient with a 68 CAG repeat,[19] and we observed a similar effect (**Figure 1d**). Transfection with a miR-298 inhibitor, an antisense RNA oligonucleotide that inhibits endogenous miR-298, resulted in an increase in AR65Q protein levels in the MN1 cells, suggesting that the effect is specific (**Figure 1e**). The discrepancies in the results from MN1 AR24Q and AR65Q could be ascribed to the different levels of baseline AR expression between the cell lines, which are lower in the mutant clone (**Figure 1c**,**e**). AR mRNA levels were also reduced by miR-298 in MCF7 cells (**Supplementary Figure S2**). To determine whether the decrease in the AR mRNA was due to the enhancement of mRNA degradation or a decrease in mRNA synthesis, we assessed AR mRNA turnover by incubating the cells with the transcription blocker actinomycin D: miR-298 significantly enhanced AR mRNA degradation compared to scrambled control (**Figure 1f**). An XTT assay showed that cell viability in the presence of DHT was significantly increased in AR65Q MN1 cells treated with miR-298 as compared to a scrambled control with random sequence that does not affect miRNA levels (**Figure 1g**). Staurosporine treatment was used as a positive control in this experiment (**Figure 1g**).

Together, these data indicate that miR-298 reduces AR protein at least in part by promoting degradation of AR mRNA and protects against mutant AR toxicity *in vitro*.

Expression of miR-298 is altered in SBMA

Levels of endogenous miR-298 were examined in SBMA models. We found that the levels of miR-298 are reduced by approximately 50% in MN1 cells expressing AR65Q compared to AR24Q (**Figure 2a**). We next examined endogenous miR-298 levels *in vivo* in wild-type mice and in a transgenic SBMA mouse model carrying a full-length human AR with a pathologically expanded polyglutamine tract (AR97Q).[20] Real-time reverse transcription-PCR (qRT-PCR) analysis in adult wild-type C57Bl6 mice showed that miR-298 is enriched in spinal cord and brain, modestly expressed in skeletal muscle (<10% of spinal cord expression), and virtually absent in other tissues collected (**Figure 2b**). Ingenuity pathway analysis on predicted miR-298 targets showed enrichment in genes expressed in neurons and linked with neuromuscular diseases (**Supplementary Table S2**). Spinal cord and muscle, tissues that are relevant for SBMA, were then harvested at early (8 weeks) and late (16 weeks) disease stages from male mice carrying the wild-type (AR24Q) or mutant (AR97Q) AR transgene. Interestingly, miR-298 levels were reduced in muscle at late stage in AR97Q mice compared to AR24Q (**Figure 2c**). No reduction was observed in spinal cord (**Supplementary Figure S3**). No difference was found in either tissue in the levels of the primary miR-298 (pri-miR-298) (**Figure 2c** and **Supplementary Figure S3**) and of miR-296, a miRNA which arises from the same transcript as miR-298 (not shown), indicating a specific dysregulation in levels of mature miR-298 in SBMA.

AAV9-mediated delivery of miR-298 in wild-type mice

In order to increase expression levels of miR-298 *in vivo*, we used a delivery system with an adeno-associated virus 9 (AAV9) dual promoter vector in a back-to-back configuration for simultaneous expression of either miR-298 (AAV9-miR-298) or a nonspecific miRNA, miR-mock (AAV-miR-mock), and green fluorescent protein (GFP) (**Figure 3a**). The AAV9 vector was chosen because it efficiently crosses the blood–brain barrier and has been shown to transduce neurons.[21] To characterize the efficiency of viral delivery in mice, we injected a viral load of 10^{11} vg of AAV9-miR-298 or AAV-miR-mock in C57Bl6 mice by single tail–vein injection at 5 weeks of age. Two weeks after the administration, we observed widespread expression of human miR-298 in skeletal muscle, which peaked 8 weeks after the injection (six times more than baseline) in the mice treated with AAV9-miR-298 (**Figure 3b**). In spinal cord, an increase in miR-298 expression was observed only after 4 weeks and peaked 12 weeks after the injection (15 times more than baseline) (**Figure 3c**). The virus delivered by intravenous injection efficiently and homogenously transduced the quadriceps muscle (**Figure 3d**) and the spinal cord (**Figure 3e**), as indicated by GFP expression levels in transverse sections of lumbar spinal cord and quadriceps muscle from treated adult wild-type mice. The widespread transduction of the AAV vector in motor neurons was confirmed by colocalization of staining for GFP and the motor neuron marker choline acetyltransferase (ChAT) (**Figure 3f** and **Supplementary Figure S4**). Human miR-298 levels were undetectable in infected mice 20 weeks after administration (not shown).

MiR-298 overexpression ameliorates disease phenotype in SBMA mice

To determine the effects of miR-298 expression in SBMA, a cohort of male AR97Q mice was randomized to receive either AAV-miR-mock or AAV-miR-298 with the same dosage regimen used for the wild-type mice. Ten weeks after the injection, levels of human miR-298 were >5-fold higher in muscle (**Supplementary Figure S5**) and >15-fold higher in spinal cord (**Supplementary Figure S6**) compared to mock-treated mice, in line with the levels in wild-type mice at the same age (**Figure 3b**,**c**). By 16 weeks of age, miR-298-treated mice showed reduced overall atrophy compared to mock-treated littermates (**Figure 4a**).

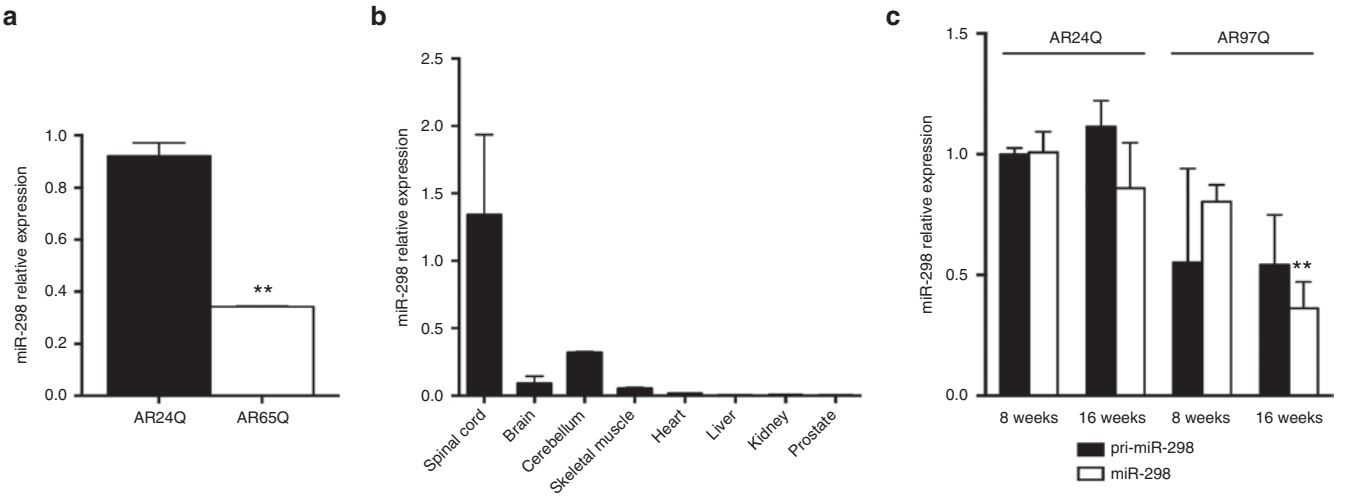

Figure 2 MiR-298 expression is altered in *in vitro* and *in vivo* models of spinal and bulbar muscular atrophy (SBMA). (**a**) Endogenous miR-298 levels were assessed by qRT-PCR using total RNA extracted from AR24Q and AR65Q MN1 cells, in the presence of dihydrotestosterone (10 nmol/l). Transcript levels were normalized to snoRNA202 (n = 5). $^{**}P < 0.01$. (**b**) Endogenous miR-298 levels were assessed by qRT-PCR using total RNA extracted from the indicated tissues of 16-week-old wild-type mice. Transcript levels were normalized to snoRNA202 (n = 3 per group). (**c**) Endogenous miR-298 and pri-miR-298 levels were assessed by qRT-PCR using total RNA extracted from the quadriceps femoris of AR24Q and AR97Q SBMA mice of the indicated ages. Transcript levels were normalized to snoRNA202 (n = 5 per group). $^{**}P < 0.01$. qRT-PCR, real-time reverse transcription-PCR.

MiR-298 administration, although not increasing overall survival (**Supplementary Figure S7**), resulted in significant reduction of the weight loss (**Figure 4b**) and improved motor function (**Figure 4c**) as assessed by the hanging wire test; body weight and muscle strength of mock-treated mice declined rapidly after 10 weeks of age (**Figure 4b**,**c**). Levels of human AR mRNA were reduced by 50% in both skeletal muscle and spinal cord extracts of miR-298-treated mice compared to mock-treated mice, indicating that miR-298 is able to target AR expression *in vivo* (**Figure 4d**,**e**). We next investigated whether AAV-delivery of miR-298 also has an effect on AR protein levels and aggregates in the SBMA mice. Here, we define aggregates as high-molecular weight oligomers that can be detected as a smear in the stacking portion of sodium dodecyl sulfate (SDS)–polyacrylamide gels, as previously described.[22,23] Western blot analysis showed that miR-298 reduces the accumulation of both monomeric and aggregated mutant AR in the skeletal muscle of AR97Q mice (**Figure 4f**). A strong linear inverse relationship was found between the miR-298 fold change and AR protein levels in muscle, indicating a dose–response effect of miR-298 on AR expression (**Figure 4g**). We next investigated the effects of miR-298 treatment on SBMA pathology. Quadriceps muscles from 16-week-old SBMA mice treated with miR-298 or mock were collected for histopathological analyses. Muscle cross-sections stained with hematoxylin and eosin and nicotinamide adenine dinucleotide showed the presence of angulated myofibers, grouped atrophic fibers, and enlarged fibers with central nuclei in mock-treated AR97Q mice, as previously reported[23] (**Figure 4h**). These neuropathic and myopathic changes were reduced in miR-298 treated mice (**Figure 4h**).

A pathological hallmark in polyglutamine diseases is the formation of nuclear and cytoplasmic inclusions of polyglutamine-containing proteins in affected cells. Immunohistological staining of mouse tissues with 1C2 antibody, which recognizes the expanded polyglutamine,[24] showed a marked reduction in 1C2-positive nuclear accumulation in the anterior horn of the lumbar spinal cord and in the skeletal muscle of miR-298 treated compared with mock-treated mice (**Figure 4i**,**j** and **Supplementary Figures S8 and S9**). To examine the effects of miR-298 on motor neurons of SBMA mice, we analyzed the anterior horn of lumbar spinal cord transverse sections using Nissl staining and blindly assessed motor neuron number and cross-sectional area (**Figure 4k**). The average cross-sectional area of motor neurons was significantly increased compared to mock-treated mice, suggesting a healthier status (**Figure 4l**). AAV9-miR treatment did not affect the number of motor neurons in these mice (**Supplementary Figure S10**), however, unlike in patients, disease pathology is not associated with a significant loss of motor neurons in this mouse model.[20] Spinal cord sections from both treatment groups showed a similar, low baseline level of glial fibrillary acidic protein-positive astrocytes (**Supplementary Figure S11**); in addition, staining for the microglial marker Iba1 was also similar in all mouse groups, showing that mir-298 treatment did not induce gliosis (**Supplementary Figure S11**).

Collectively, these results show that systemic administration of AAV9-miR-298 efficiently transduces muscle and spinal cord, downregulates AR expression *in vivo*, and ameliorates the disease phenotype in SBMA mice.

DISCUSSION

In the last decade, miRNAs have become a viable option for the mitigation of disease manifestations *in vivo*, and many miRNA-based therapies, both mimics and inhibitors, are currently in preclinical or clinical development for a variety of conditions, including polyglutamine diseases.[25–28] Compared to other RNA inhibition strategies, miRNAs are likely to be less toxic and less immunogenic, given that they make use of naturally occurring RNA interference mechanisms and can be easily delivered into cells due to their small size.[29] A miRNA approach using miR196a overexpression

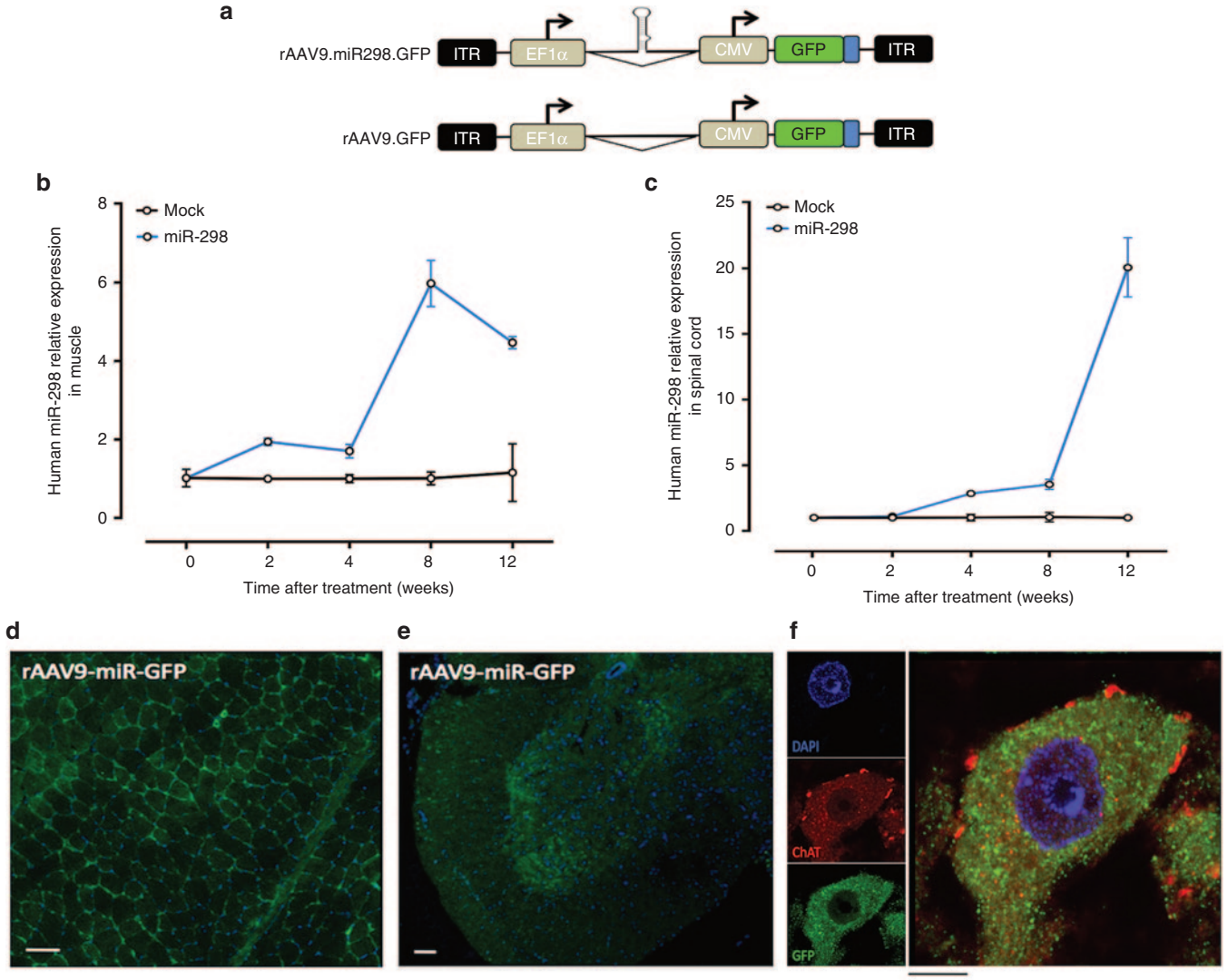

Figure 3 AAV9-mediated delivery of miR-298 in mice. (**a**) Schematic representation of the AAV plasmid constructs used. Dual promoter AAV vector plasmids contained an expression cassette consisting of a human elongation factor-1α (EIF1α) promoter followed by miR-298 or mock sequence and human cytomegalovirus (CMV) promoter followed by cDNA encoding GFP. (**b**) Temporal changes in the levels of human miR-298 expression in the quadriceps femoris and (**c**) spinal cord of wild-type mice, after single tail-vein injection at 5 weeks of age of AAV9-mock-GFP of AAV9-miR-298-GFP (n = 2 per group). (**d**) Representative transverse sections of the right quadriceps femoris and (**e**) lumbar spinal cord of miR-298-treated wild-type mice, stained with GFP (green) and DAPI (blue). Original magnification, ×10. Scale bar, 100 µm. (**f**) A representative motor neuron of miR-298-treated wild-type mouse, stained with GFP (green), ChAT (red) and DAPI (blue). Original magnification, ×40. Scale bar, 10 µm.

has recently shown some benefit in SBMA models;[15] in this study, AR suppression was indirectly achieved via silencing of the RNA binding protein CELF2. MiR196a has been shown to play a role in the progression of a variety of cancers,[30,31] and this may raise concerns about the safety of bringing this agent into the clinic.

Here, we identified a miRNA, miR-298, that directly targets and suppresses AR in cell culture and in an animal model of SBMA. MiR-298 is a poorly characterized miRNA known to be expressed in brain.[16] Interestingly, an increase in serum levels of miR-298 has been detected in mice and subjects with androgen-responsive prostate cancer, suggesting a role of miR-298 in androgen receptor biology.[32]

First, we determined its expression levels in various tissues from adult wild-type mice. We found that miR-298 is particularly enriched in spinal cord and brain, and at lower levels in muscle, tissues that are relevant in SBMA pathogenesis, and virtually absent in all other tested tissues. The endogenous levels of miR-298 were reduced in muscle tissue and, although not significantly, in spinal cord of SBMA mice in late-stage disease. It is noteworthy that this mouse model shows a muscle pathology with limited involvement of motor neurons in spinal cord, suggesting a functional correlation with the disease state. No changes were found in the pri-miR-298, the upstream transcript in the microRNA biogenesis pathway, ruling out decreased transcription as a possible explanation. To evaluate the specificity of this finding, we measured the abundance of miR-296 in the same tissues, and found no difference in SBMA compared to wild-type mice (data not shown). Both miR-298 and miR-296 arise from a long, antisense transcript, Nespas, a noncoding macroRNA with a promoter in the imprinting control region, a discrete DNA

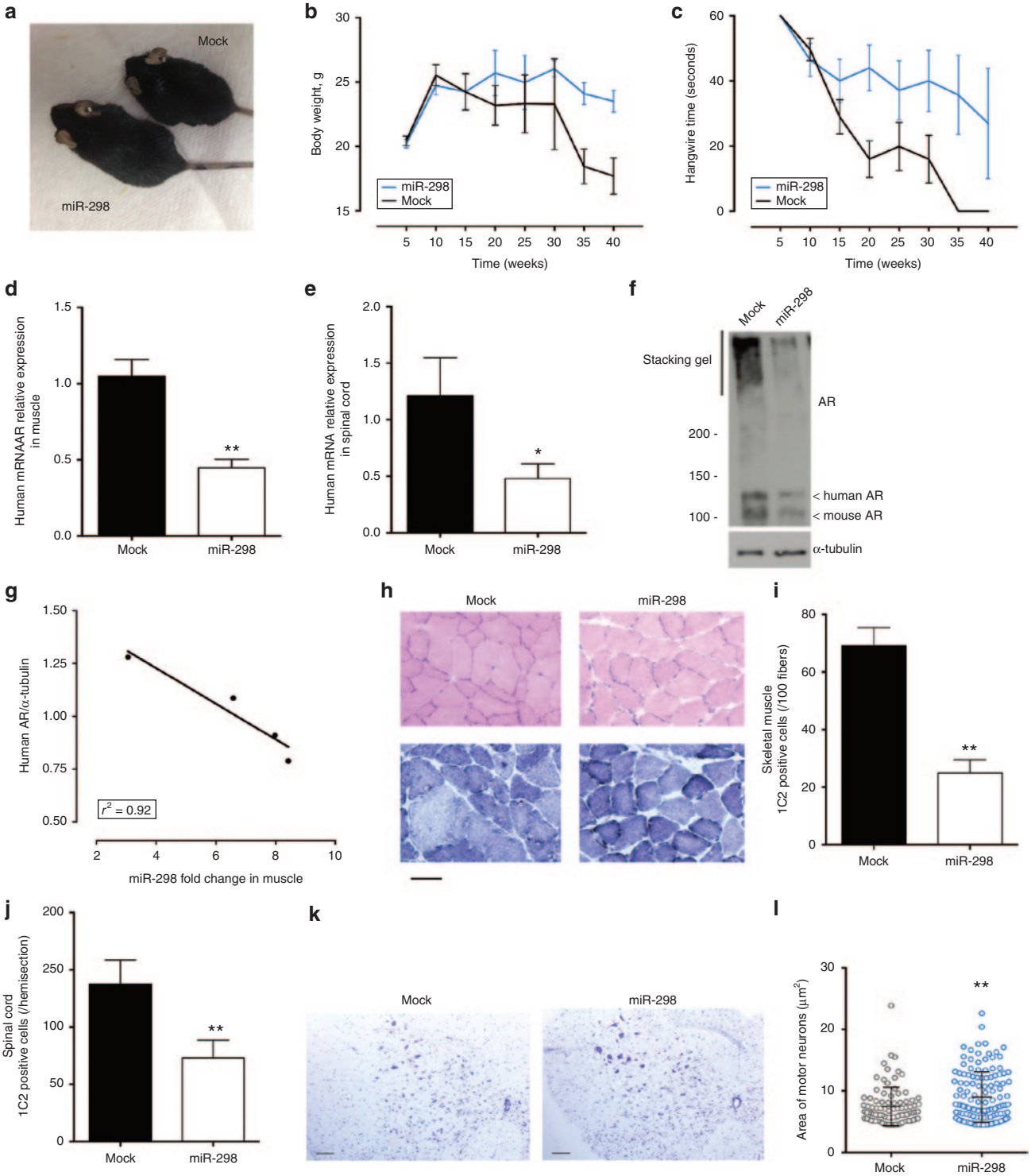

Figure 4 MiR-298 overexpression ameliorates disease phenotype in spinal and bulbar muscular atrophy (SBMA) mice. (**a**) A representative photograph of a 16-week-old AR97Q mock-treated mouse (right) and an age-matched AR97Q miR-298-treated mouse (left). (**b**) Body weight and (**c**) hanging wire performance of SBMA mice ($n = 15$ per group). $P < 0.01$, two-way analysis of variance. (**d**) AR expression was assessed by real-time reverse transcription-PCR using total RNA extracted from quadriceps muscle and (**e**) lumbar spinal cord of 16-week-old AR97Q mice. Transcript levels were normalized to snoRNA202 ($n = 5$ per group). *$P < 0.05$, **$P < 0.01$. (**f**) Representative western blot of AR protein levels in quadriceps femoris of 16-week-old AR97Q mice. AR was detected with H-280 antibody. α-tubulin was used as a loading control. Shown is one experiment representative of 4. (**g**) Regression analysis between the miR-298 fold change and AR protein levels in skeletal muscle of miR-298-treated ASBMA mice. (**h**) Representative pictures of hematoxylin and eosin (H&E) (top) and nicotinamide adenine dinucleotide (NADH) (bottom) staining of skeletal muscle transverse sections of the right quadriceps femoris of 16-week-old AR97Q mice. Original magnification, ×40. Scale bar, 100 μm. (**i**) Quantification of 1C2-positive cells in skeletal muscle of the right quadriceps femoris and (**j**) lumbar section of spinal cord of 16-week-old AR97Q mice ($n = 5$ per group). **$P < 0.01$. (**k**) Representative pictures of Nissl-stained transverse sections of lumbar spinal cords of 16-week-old AR97Q mice. Original magnification, ×20. Scale bar, 100 μm. (**l**) Quantification of the areas of motor neurons in transverse sections of lumbar spinal cords of 16-week-old AR97Q mice ($n = 5$ per group). **$P < 0.01$.

sequence with cis-acting regulatory elements which controls parental-specific expression of a subset of genes.[33] Both miRNAs show imprinted expression and are expressed from the paternally derived allele, but not the maternal allele,[33] suggesting a parental-specific regulation of their target genes.

We next proceeded to test the efficacy of miR-298 overexpression in SBMA transgenic mice. As a delivery tool we chose adeno-associated virus (AAV), which is a vector of choice in gene therapy,[34] due to its safety, low immunogenicity, long-term gene transfer, and broad spectrum of tropism in dividing and nondividing cells.[35] Currently, recombinant AAV (rAAV) vectors are being evaluated in phase 1/2 clinical trials for a variety of diseases, including cystic fibrosis, Parkinson's disease, muscular dystrophy, and Leber's congenital amaurosis.[36] A rAAV vector expressing lipoprotein lipase was recently approved for treatment of patients with lipoprotein lipase deficiency in Europe.[37] Among the different serotypes, we selected rAAV9, which, perhaps because of its capsid composition,[38] has robust and sustained transduction throughout the central nervous system in animal models with peripheral administration.[39,40] Usually greater neuronal transduction has been observed in neonatal animals compared to adult animals, where glial transduction prevails.[41,42] This discrepancy has been attributed to factors such as differences in extracellular matrix composition, neuron-to-glia ratio, and blood–brain barrier maturity.[41,42]

Peripheral injections at 5 weeks of age led to increased miR-298 expression in spinal cord and muscle after 2–4 weeks, in conjunction with the appearance of the first signs of disease manifestations in this mouse model.[20] Delayed transduction is well documented when using single-stranded genome AAV vectors and is likely due to the rate-limiting step involving the *de novo* synthesis of the second DNA strand. Non-cell-autonomous neurotoxicity has been increasingly recognized as a component of SBMA and other neurodegenerative disorders.[43] In particular, muscle has been shown to be primarily involved in SBMA pathogenesis,[44,45] therefore, therapies simultaneously targeting motor neurons in spinal cord and muscle, may be an ideal strategy for this disease.

Each miRNA targets many gene transcripts, and the rules governing imperfectly complementary miRNA-target interactions are not completely understood, which poses a risk to the safety of this approach. Nevertheless, the direct downstream targets of a single miRNA are commonly related genes that function in convergent cellular pathways, potentially resulting in a synergistic effect. Addressing these issues carefully is important in translating a miRNA strategy into a safe and effective therapy. Although the biological significance of the miR-298-mediated suppression of targets other than AR still remains to be demonstrated, treatment in SBMA mice resulted in increased body weight, better motor performance and amelioration of the histopathological features in muscle and spinal cord. Viral delivery of miR-298 did not alter life expectancy and did not lead to signs of increased gliosis, microglial activation, or decrease motor neuron number in SBMA mice. The lack of effect on survival could be ascribed to the fact that human miR-298 becomes undetectable in mouse tissues 20 weeks after administration, at which point more than 50% of the mice in our cohort were still alive.

A number of solutions are now being implemented to address these concerns,[46] such as designing RNAi sequences that minimize interaction with off-target transcripts and using non-canonical miRNAs, such as mirtrons, which bypass the microprocessor complex.[47] Extensive long-term safety and tolerability studies are critical to assess the effects of long-term transcript suppression which may exacerbate symptoms of loss of function in SBMA. With a growing understanding of AAV as a vector and of the mechanisms of RNAi, this approach has the potential to safely and effectively treat not only SBMA but also other neurodegenerative disorders caused by toxic proteins.

MATERIALS AND METHODS

Cell culture. Human fibroblasts, MN1 and MCF7 cells were maintained in Dulbecco's Modified Eagle's medium containing 10% fetal bovine serum in a humidified chamber at 37 °C and 5% CO_2. The cells were plated before transfection in six-well plates. The following day, 150 pmoles of miRNA duplexes were transfected using Lipofectamine 2000 (Invitrogen, Carlsbad, CA) according to the manufacturer's instructions, and cells were cultured in Dulbecco's Modified Eagle's medium with 10% fetal bovine serum for 48 hours. The miRNA mimics hsa-miR-298 (MC12574) and mmu-miR-298 (MC12525), the miRNA inhibitor mmu-miR-298 (AM12525), and negative controls (AM17110 and 4464076, respectively) were obtained from Applied Biosystems (Foster City, CA).

Luciferase constructs and assays. First, 4126 bp of the human AR-3'UTR sequence was amplified by polymerase chain reaction and cloned in the psicheck2 plasmid (Promega, Madison, WI) downstream from the renilla luciferase gene. The same plasmid also contains firefly luciferase to normalize transfection efficiency. The following primers, designed to have XhoI and NotI restriction sites at 5′ and 3′ ends of polymerase chain reaction (PCR) products, were used: 5′-AGCTGCTCGAGGCATCAGTTCACTTTTGACCTG-3′ (forward primer) and 5′-ACCTGCGGCCGCACATGAAAACCACTCCCTTGG-3′ (reverse primer). Mutations were made by altering two bases within the seed region of the predicted miRNA binding site using QuickChange II XL Site-directed Mutagenesis Kit (Roche, Indianapolis, IN). Luciferase assays were performed on 10 µl of MCF7 cell lysate in 96-well assay plates using the dual luciferase assay (Promega) according to the manufacturer's instructions in a Victor Wallac plate reader (PerkinElmer, Waltham, MA).

Cell death assay. Cell proliferation and viability (XTT assay) was measured using the Cell Proliferation Kit II (Roche Diagnostics). MN1 cells were transfected with 150 pmoles of miRNA duplexes and cultured in serum-free media, DHT (10 nmol/l), and aphidicolin (1 µg/ml, Calbiochem) in 96-well plates. Treatment with 1 µmol/l staurosporine for 6 hours (Sigma) was used as a positive control. Absorbance was measured at time 0, 48, and 72 hours after transfection at 450 and 650 nm wavelengths using a microtiter plate reader, as per manufacturer's instructions.

Animal model. Wild-type C57Bl6 and SBMA mice were used for the experiments. The SBMA mice, which express a transgene consisting of human AR with a 24 (AR24Q) or 97 (AR97Q) glutamine repeat, have been described.[20] All experiments were performed in the F1 generation derived from crossing the AR97Q line in a C57Bl6 background to BDF1 mice. The mice were genotyped by PCR with tail DNA as previously described,[20] by using a REDExtract-N-Amp Tissue PCR kit (Sigma, St. Louis, MO) according to the manufacturer's instructions. Dual promoter AAV vector plasmids containing an expression cassette consisting of a human elongation factor-1α (EIF1α) promoter followed by miR-298 or mock sequence and human cytomegalovirus (CMV) promoter followed by cDNA encoding GFP, were provided by SignaGen Laboratories (Rockville, MD). A viral load of 10^{11} vector genomes (vg) of each of these constructs was injected into the tail veins of AR97Q mice at 5 weeks of age. Body weight and grip strength determined using hanging wire test were recorded weekly

as previously described.[22] The treatments were administered and analyses performed by blinded investigators.

Taqman quantitative PCR analysis. Total RNA was extracted from cultured cells or mouse tissues using Qiazol reagent (QIAGEN, Gaithersburg, MD) and reverse-transcribed with the TaqMan MicroRNA Reverse Transcription kit according to manufacturer's instructions. Transcript levels were determined by qRT-PCR using TaqMan reagents with an ABI9900 Sequence Detector System using the threshold cycle method and snoRNA202 (001232) as a reference gene. The Taqman assays used were has-miR-298 (002190), mmu-miR-298 (AM12525), and mmu-pri-miR-298 (Mm03306612_pri), all from Life Technologies (Grand Island, NY).

RNA stability assay. We added 10 mg/ml actinomycin D, a potent inhibitor of mRNA synthesis, to MCF7 cells at 24 hours after transfection of RNAi molecules. The total RNA was extracted from the cells at 0, 3, 6, and 12 hours after treatment, and the RNA was then subjected to qRT-PCR as described above. The data are presented as values relative to the levels of expression detected in the transfected cells harvested at the time of actinomycin D treatment.

Protein analyses. For quantification of proteins, cells were washed twice in ice-cold PBS and scraped in 150 µl lysis buffer (150 mmol/l NaCl, 6 mmol/l Na_2HPO_4, 12 mmol/l NaH_2PO_4, 5 mmol/l ethylenediaminetetraacetic acid, 1% Na-deoxycholate, 1% Triton X-100, 0.1% sodium dodecyl sulfate) plus protease inhibitor cocktail (Roche Diagnostics). The lysates were sonicated and centrifuged at 15,700 g for 10 minutes at 4 °C. Cell lysates were denatured at 95 °C in 4× sample buffer (60 mmol/l Tris, pH 6.8, 2% SDS, 25% glycerol, 0.1% bromophenol blue, 20% β-mercaptoethanol) and processed for 10% SDS–polyacrylamide gel electrophoresis (SDS–PAGE), and electro-transferred to polyvinylidene fluoride membrane (Millipore, Billerica, MA). Quadriceps muscles and spinal cord were dissected and snap frozen in liquid nitrogen. The tissue samples were processed with a polytron homogenizer in ice-cold homogenization radioimmunoprecipitation assay buffer (150 mmol/l NaCl, 50 mmol/l Tris, 2 mmol/l ethylenediaminetetraacetic acid, 1% sodium deoxycholate, 0.5% Triton X-100, 0.1% SDS) containing 1× protease inhibitor and phosphatase inhibitor cocktails (Roche). Homogenates were sonicated and precleaned at 4,000g for 10 minutes at 4 °C. The soluble fraction was collected and protein concentration was determined using Bradford reagent (Bio-Rad, Hercules, CA). Membranes were probed with antibodies for AR (1:1,000; H-280, sc-13062, Santa Cruz, Santa Cruz, CA) and α-tubulin (1:5,000; T6199, Sigma-Aldrich) in Tris-buffered saline and 5% (weight/vol) non-fat dry milk overnight at 4 °C. Immunoreactivity was detected using peroxidase-conjugated AffiniPure Goat Anti-Rabbit or Anti-Mouse IgG (1:5,000; Jackson ImmunoResearch, West Grove, PA), and visualized using chemiluminescence reagent (Perkin-Elmer) following the manufacturer's instructions.

Immunohistochemistry and histopathology. Quadriceps muscles from 16-week-old mice were snap frozen in isopentane. Sections of unfixed muscle tissue were cut at 8 µm in a -20 °C cryostat and processed for hematoxylin and eosin, and nicotinamide adenine dinucleotide staining. For immunofluorescence analysis, sections were fixed with 4% paraformaldehyde and incubated overnight at 4 °C with GFP (1:1,000; ab290, Abcam, San Francisco, CA). To visualize the inclusions, fixed tissue sections were stained with 1C2 antibody (1:20,000; EMD Millipore) followed by biotinylated mouse IgG (R&D Systems, Minneapolis, MN), streptavidin-HRP and 3,3′-diaminobenzidine substrate (Life Technologies); nuclei were counterstained using hematoxylin. For each mouse, the number of 1C2-positive nuclei was determined in at least 500 muscle fibers in randomly selected views. Paraffin-embedded spinal cords were serially sectioned at 6-µm steps, mounted on slides and processes for Nissl staining. Images of 10 contiguous sections, 100 µm apart (original magnification 10×), were analyzed. Motor neurons were identified in the anterior horn of the spinal cord as cells positive for Nissl staining, with clear nucleus and nucleolus, and a maximum diameter greater than 25 µm. Counting was performed in blinded fashion. For immunofluorescence analysis, sections were fixed with 4% paraformaldehyde and incubated overnight at 4 °C with antibodies for GFP (1:1,000; ab290, Abcam), choline acetyltransferase (ChAT; 1:1,000; AB144P, Chemicon, Billerica, MA), anti-glial fibrillary acidic protein (1:500; MAB360, Chemicon), and ionized calcium-binding adapter molecule 1 (Iba1; 1:1,000; 019-19741, Wako, Richmond, VA). Digital images were captured with a Zeiss Axiovert 100 M microscope and analyzed with NIS Elements software for total cross-sectional area.

Experimental design. All experiments were conducted blindly by third party concealment of treatments with individually uniquely coded vials. Order of treatments was randomized.

Study approval. The study was carried out in accordance with the National Institute of Health Guide for the Care and Use of Laboratory Animals and was approved by the National Institute of Neurological Disorders and Stroke Animal Care Committee.

Statistics. All experiments were carried out at least three times independently. Western blots were quantified using the Image J software package (http://imagej.nih.gov/ij/). Statistical significance of differences between control and experimental values was determined using two-tailed Student's t test or two-way analysis of variance, where indicated. A log-rank test was used to compare Kaplan-Meier survival. All data are reported as means ± standard errors, and statistical significance is indicated by asterisks. *P* values of less than 0.05 were considered significant.

SUPPLEMENTARY MATERIAL

Table S1. List of evolutionarily conserved predicted miRNA-binding sites in the 3′UTR of human AR using the miRanda, miRDB, miRWalk, and Targetscan databases.

Table S2. Ingenuity pathway analysis was performed on predicted targets of miR-298 using the Targetscan v6 algorithm.

Figure S1. AR/tubulin fold change protein expression in MCF7 cells transfected with the indicated miRNAs or a scrambled control (n = 3).

Figure S2. AR expression was assessed in presence of DHT (10 nM) by qRT-PCR using total RNA extracted from MCF7 cells treated with scramble (scr) or miR-298 (n = 5).

Figure S3. Endogenous miR-298 and pri-miR-298 levels were assessed by qRT-PCR using total RNA extracted from the lumbar spinal cord of AR24Q and AR97Q SBMA mice of the indicated ages.

Figure S4. Representative pictures of the anterior horn of the lumbar spinal cord of miR-298-treated wild-type mouse, stained with GFP (green), ChAT (red) and DAPI (blue).

Figure S5. Human miR-298 levels were assessed by qRT-PCR using total RNA extracted from the quadriceps femoris of 16-week-old AR97Q SBMA mice treated with AAV-miR-mock (mock) or AAV-miR-298 (miR-298).

Figure S6. Human miR-298 levels were assessed by qRT-PCR using total RNA extracted from the lumbar spinal cord of 16-week-old AR97Q SBMA mice treated with AAV-miR-mock (mock) or AAV-miR-298 (miR-298).

Figure S7. Kaplan-Meier survival curves of mice treated with AAV-miR-mock or AAV-miR-298 (n = 15 per group).

Figure S8. Representative pictures of 1C2 staining of the right quadriceps femoris of 16-week-old mock-treated (left) and miR-treated (right) AR97Q mice Original magnification, ×40.

Figure S9. Representative pictures of 1C2 staining of lumbar spinal cords of 16-week-old mock-treated (left) and miR-treated (right) AR97Q mice.

Figure S10. The average number of the motor neurons of the lumbar spinal cord obtained from miR-298-treated mice were compared with that of mock-treated mice (n = 5).

Figure S11. Representative pictures of a section of lumbar spinal cord of mock-treated and miR-298-treated SBMA mice stained with GFP (green), microglia marker Iba1 (red), astrocyte marker GFAP (yellow), and DAPI (blue).

ACKNOWLEDGMENTS

The authors thank SignaGen Laboratories (Rockvile, MD, USA) for the AAV9 virus production. This research was supported by the Intramural Research Program of the National Institute of Neurological Disorders and Stroke, NIH. Philip R. Lee was supported by funds from the Division of Intramural Research of NICHD. Carlo Rinaldi was supported by a fellowship from the Association Française contre les Myopathies. The authors declare no conflict of interest.

REFERENCES

1. Zoghbi, HY and Orr, HT (2000). Glutamine repeats and neurodegeneration. *Annu Rev Neurosci* **23**: 217–247.
2. Orr, HT (2012). Polyglutamine neurodegeneration: expanded glutamines enhance native functions. *Curr Opin Genet Dev* **22**: 251–255.
3. Szebenyi, G, Morfini, GA, Babcock, A, Gould, M, Selkoe, K, Stenoien, DL *et al.* (2003). Neuropathogenic forms of huntingtin and androgen receptor inhibit fast axonal transport. *Neuron* **40**: 41–52.
4. Katsuno, M, Adachi, H, Minamiyama, M, Waza, M, Tokui, K, Banno, H *et al.* (2006). Reversible disruption of dynactin 1-mediated retrograde axonal transport in polyglutamine-induced motor neuron degeneration. *J Neurosci* **26**: 12106–12117.
5. Morfini, G, Pigino, G, Szebenyi, G, You, Y, Pollema, S and Brady, ST (2006). JNK mediates pathogenic effects of polyglutamine-expanded androgen receptor on fast axonal transport. *Nat Neurosci* **9**: 907–916.
6. Ranganathan, S, Harmison, GG, Meyertholen, K, Pennuto, M, Burnett, BG and Fischbeck, KH (2009). Mitochondrial abnormalities in spinal and bulbar muscular atrophy. *Hum Mol Genet* **18**: 27–42.
7. Yu, YC, Kuo, CL, Cheng, WL, Liu, CS and Hsieh, M (2009). Decreased antioxidant enzyme activity and increased mitochondrial DNA damage in cellular models of Machado-Joseph disease. *J Neurosci Res* **87**: 1884–1891.
8. Ambros, V (2004). The functions of animal microRNAs. *Nature* **431**: 350–355.
9. Ghildiyal, M and Zamore, PD (2009). Small silencing RNAs: an expanding universe. *Nat Rev Genet* **10**: 94–108.
10. Hayes, J, Peruzzi, PP and Lawler, S (2014). MicroRNAs in cancer: biomarkers, functions and therapy. *Trends Mol Med* **20**: 460–469.
11. Bilen, J, Liu, N, Burnett, BG, Pittman, RN and Bonini, NM (2006). MicroRNA pathways modulate polyglutamine-induced neurodegeneration. *Mol Cell* **24**: 157–163.
12. Lee, Y, Samaco, RC, Gatchel, JR, Thaller, C, Orr, HT and Zoghbi, HY (2008). miR-19, miR-101 and miR-130 co-regulate ATXN1 levels to potentially modulate SCA1 pathogenesis. *Nat Neurosci* **11**: 1137–1139.
13. Packer, AN, Xing, Y, Harper, SQ, Jones, L and Davidson, BL (2008). The bifunctional microRNA miR-9/miR-9* regulates REST and CoREST and is downregulated in Huntington's disease. *J Neurosci* **28**: 14341–14346.
14. Liu, N, Landreh, M, Cao, K, Abe, M, Hendriks, GJ, Kennerdell, JR *et al.* (2012). The microRNA miR-34 modulates ageing and neurodegeneration in Drosophila. *Nature* **482**: 519–523.
15. Miyazaki, Y, Adachi, H, Katsuno, M, Minamiyama, M, Jiang, YM, Huang, Z *et al.* (2012). Viral delivery of miR-196a ameliorates the SBMA phenotype via the silencing of CELF2. *Nat Med* **18**: 1136–1141.
16. Boissonneault, V, Plante, I, Rivest, S and Provost, P (2009). MicroRNA-298 and microRNA-328 regulate expression of mouse beta-amyloid precursor protein-converting enzyme 1. *J Biol Chem* **284**: 1971–1981.
17. Dweep, H, Sticht, C, Pandey, P and Gretz, N (2011). miRWalk–database: prediction of possible miRNA binding sites by "walking" the genes of three genomes. *J Biomed Inform* **44**: 839–847.
18. Brooks, BP, Paulson, HL, Merry, DE, Salazar-Grueso, EF, Brinkmann, AO, Wilson, EM *et al.* (1997). Characterization of an expanded glutamine repeat androgen receptor in a neuronal cell culture system. *Neurobiol Dis* **3**: 313–323.
19. Grunseich, C, Kats, IR, Bott, LC, Rinaldi, C, Kokkinis, A, Fox, D *et al.* (2014). Early onset and novel features in a spinal and bulbar muscular atrophy patient with a 68 CAG repeat. *Neuromuscul Disord* **24**: 978–981.
20. Katsuno, M, Adachi, H, Kume, A, Li, M, Nakagomi, Y, Niwa, H *et al.* (2002). Testosterone reduction prevents phenotypic expression in a transgenic mouse model of spinal and bulbar muscular atrophy. *Neuron* **35**: 843–854.
21. Gray, SJ, Choi, VW, Asokan, A, Haberman, RA, McCown, TJ and Samulski, RJ (2011). Production of recombinant adeno-associated viral vectors and use in *in vitro* and *in vivo* administration. *Curr Protoc Neurosci* **Chapter 4**: Unit 4.17.
22. Li, M, Chevalier-Larsen, ES, Merry, DE and Diamond, MI (2007). Soluble androgen receptor oligomers underlie pathology in a mouse model of spinobulbar muscular atrophy. *J Biol Chem* **282**: 3157–3164.
23. Rinaldi, C, Bott, LC, Chen, KL, Harmison, GG, Katsuno, M, Sobue, G *et al.* (2012). Insulinlike growth factor (IGF)-1 administration ameliorates disease manifestations in a mouse model of spinal and bulbar muscular atrophy. *Mol Med* **18**: 1261–1268.
24. Trottier, Y, Lutz, Y, Stevanin, G, Imbert, G, Devys, D, Cancel, G *et al.* (1995). Polyglutamine expansion as a pathological epitope in Huntington's disease and four dominant cerebellar ataxias. *Nature* **378**: 403–406.
25. Elmén, J, Lindow, M, Schütz, S, Lawrence, M, Petri, A, Obad, S *et al.* (2008). LNA-mediated microRNA silencing in non-human primates. *Nature* **452**: 896–899.
26. Nana-Sinkam, SP and Croce, CM (2013). Clinical applications for microRNAs in cancer. *Clin Pharmacol Ther* **93**: 98–104.
27. Rodríguez-Lebrón, E, Costa, Mdo C, Costa, Md, Luna-Cancalon, K, Peron, TM, Fischer, S *et al.* (2013). Silencing mutant ATXN3 expression resolves molecular phenotypes in SCA3 transgenic mice. *Mol Ther* **21**: 1909–1918.
28. Keiser, MS, Geoghegan, JC, Boudreau, RL, Lennox, KA and Davidson, BL (2013). RNAi or overexpression: alternative therapies for Spinocerebellar Ataxia Type 1. *Neurobiol Dis* **56**: 6–13.
29. Huang, F, Zhang, L, Long, Z, Chen, Z, Hou, X, Wang, C *et al.* (2014). miR-25 alleviates polyQ-mediated cytotoxicity by silencing ATXN3. *FEBS Lett* **588**: 4791–4798.
30. Maru, DM, Singh, RR, Hannah, C, Albarracin, CT, Li, YX, Abraham, R *et al.* (2009). MicroRNA-196a is a potential marker of progression during Barrett's metaplasia-dysplasia-invasive adenocarcinoma sequence in esophagus. *Am J Pathol* **174**: 1940–1948.
31. Hui, AB, Shi, W, Boutros, PC, Miller, N, Pintilie, M, Fyles, T *et al.* (2009). Robust global micro-RNA profiling with formalin-fixed paraffin-embedded breast cancer tissues. *Lab Invest* **89**: 597–606.
32. Selth, LA, Townley, S, Gillis, JL, Ochnik, AM, Murti, K, Macfarlane, RJ *et al.* (2012). Discovery of circulating microRNAs associated with human prostate cancer using a mouse model of disease. *Int J Cancer* **131**: 652–661.
33. Robson, JE, Eaton, SA, Underhill, P, Williams, D and Peters, J (2012). MicroRNAs 296 and 298 are imprinted and part of the GNAS/Gnas cluster and miR-296 targets IKBKE and Tmed9. *RNA* **18**: 135–144.
34. Valencia-Sanchez, MA, Liu, J, Hannon, GJ and Parker, R (2006). Control of translation and mRNA degradation by miRNAs and siRNAs. *Genes Dev* **20**: 515–524.
35. Bourdenx, M, Dutheil, N, Bezard, E and Dehay, B (2014). Systemic gene delivery to the central nervous system using Adeno-associated virus. *Front Mol Neurosci* **7**: 50.
36. Mingozzi, F and High, KA (2011). Therapeutic *in vivo* gene transfer for genetic disease using AAV: progress and challenges. *Nat Rev Genet* **12**: 341–355.
37. Bryant, LM, Christopher, DM, Giles, AR, Hinderer, C, Rodriguez, JL, Smith, JB *et al.* (2013). Lessons learned from the clinical development and market authorization of Glybera. *Hum Gene Ther Clin Dev* **24**: 55–64.
38. Zhang, H, Yang, B, Mu, X, Ahmed, SS, Su, Q, He, R *et al.* (2011). Several rAAV vectors efficiently cross the blood-brain barrier and transduce neurons and astrocytes in the neonatal mouse central nervous system. *Mol Ther* **19**: 1440–1448.
39. Foust, KD, Nurre, E, Montgomery, CL, Hernandez, A, Chan, CM and Kaspar, BK (2009). Intravascular AAV9 preferentially targets neonatal neurons and adult astrocytes. *Nat Biotechnol* **27**: 59–65.
40. Duque, S, Joussemet, B, Riviere, C, Marais, T, Dubreil, L, Douar, AM *et al.* (2009). Intravenous administration of self-complementary AAV9 enables transgene delivery to adult motor neurons. *Mol Ther* **17**: 1187–1196.
41. Lowenstein, PR (2009). Crossing the rubicon. *Nat Biotechnol* **27**: 42–44.
42. Saunders, NR, Joakim Ek, C and Dziegielewska, KM (2009). The neonatal blood-brain barrier is functionally effective, and immaturity does not explain differential targeting of AAV9. *Nat Biotechnol* **27**: 804–5; author reply 805.
43. Ilieva, H, Polymenidou, M and Cleveland, DW (2009). Non-cell autonomous toxicity in neurodegenerative disorders: ALS and beyond. *J Cell Biol* **187**: 761–772.
44. Cortes, CJ, Ling, SC, Guo, LT, Hung, G, Tsunemi, T, Ly, L *et al.* (2014). Muscle expression of mutant androgen receptor accounts for systemic and motor neuron disease phenotypes in spinal and bulbar muscular atrophy. *Neuron* **82**: 295–307.
45. Lieberman, AP, Yu, Z, Murray, S, Peralta, R, Low, A, Guo, S *et al.* (2014). Peripheral androgen receptor gene suppression rescues disease in mouse models of spinal and bulbar muscular atrophy. *Cell Rep* **7**: 774–784.
46. Boudreau, RL, Spengler, RM and Davidson, BL (2011). Rational design of therapeutic siRNAs: minimizing off-targeting potential to improve the safety of RNAi therapy for Huntington's disease. *Mol Ther* **19**: 2169–2177.
47. Sibley, CR, Seow, Y, Curtis, H, Weinberg, MS and Wood, MJ (2012). Silencing of Parkinson's disease-associated genes with artificial mirtron mimics of miR-1224. *Nucleic Acids Res* **40**: 9863–9875.